Monthly Notices of the ROYAL ASTRONOMICAL SOCIETY

MNRAS **520,** 3238–3244 (2023) https://doi.org/10.1093/mnras/stad361
Advance Access publication 2023 February 2

Electron heating mechanisms at quasi-perpendicular shocks – revisited with magnetospheric multiscale measurements

Krzysztof Stasiewicz [1]★ and Bengt Eliasson[2]★

[1]*Space Research Centre, Polish Academy of Sciences, Bartycka 18A, Warsaw 00-716, Poland*
[2]*SUPA, Department of Physics, University of Strathclyde, Glasgow G4 0NG, United Kingdom*

Accepted 2023 January 27. Received 2023 January 25; in original form 2022 December 29

ABSTRACT

We demonstrate that measurements obtained from NASA's magnetospheric multiscale (MMS) mission support quasi-adiabatic electron heating in quasi-perpendicular shocks with temperature $T_{e\perp} \propto B^{1+\alpha}$, where B is the magnetic field strength and α represents departure from adiabaticity. Adiabatic heating ($\alpha = 0$) results from the conservation of magnetic moment on spatially increasing magnetic field inside the shock ramp. Negative $\alpha < 0$ is observed in most situations, where perpendicular energy gain from adiabatic heating is redistributed by interactions with waves to the parallel direction leading to a lower isotropic temperature increase. Positive α is observed when the stochastic heating of electrons is activated by the $E \times B$ wave acceleration mechanism by electrostatic waves leading to a higher temperature increase. By using test-particle simulations in a realistic shock model we have elucidated the process of stochastic wave acceleration. We have also shown the equivalence of adiabatic heating and acceleration by gradient B drift at shocks with low Mach numbers and demonstrated that the cross-shock potential does not contribute to the electron heating. Signatures of quasi-adiabatic heating and/or stochastic heating of electrons are observed in all shocks analysed with measurements by the MMS.

Key words: Shock waves – Acceleration of particles – Instabilities – Turbulence – Solar wind.

1 INTRODUCTION

Collisionless shocks in the solar wind plasma are associated with ion and electron heating and acceleration of some of the plasma particles to high energies. Early studies of the electron heating at shocks concentrated on the ratios between the downstream and upstream values. Using data from the Orbiting Geophysical Observatory (OGO) 5 satellite, Scudder, Lind & Ogilvie (1973) observed an average ratio of the downstream to upstream temperatures $T_{ed}/T_{eu} \approx 4$, whereas Bame et al. (1979) with data from the International Sun-Earth Explorer (ISEE) satellites found a ratio of 3. Thomsen et al. (1987) pointed out that these values were very low, because laboratory experiments with shocks indicated stronger electron heating by plasma instabilities. They also found bow shock crossings with $T_{ed}/T_{eu} \approx 20$ in ISEE data and strong correlation between the electron temperature increase and the kinetic energy of the incoming ions.

A strong correlation between the electron temperature and the magnetic field B as well as with the number density N is usually observed (Scudder et al. 1973; Scudder 1995; Thomsen et al. 1987; Stasiewicz & Eliasson 2020a, b). Because the electron gyroradius $r_e \approx 1$ km is small in comparison with the shock thickness ∼100 km, it is expected that the first adiabatic invariant (the magnetic moment) for electrons, but not for ions, will be conserved, leading to an adiabatic relation $T_{e\perp}(t, \mathbf{r}) = (T_{e\perp u}/B_u)B(t, \mathbf{r})$. The differential increase of the electron temperature is then $dT_{e\perp} = T_{e\perp}B^{-1}dB$.

Although the data show an increase of T_e with the increase of B at shocks, there are significant departures from proportionality, both in terms of the jump ratios, and in localized regions where strong deviations $T_{e\perp}/B \neq T_{e\perp u}/B_u$ are observed (Stasiewicz & Eliasson 2020a, b). Furthermore, the measurements generally show isotropic electron temperatures at shocks, $T_{e\parallel} \approx T_{e\perp}$, indicating that other processes, presumably waves, must be involved in isotropization (Scudder 1995; Mozer & Sundqvist 2013).

Anomalous resistivity due to ion acoustic waves, modified two-stream instability, and other cross-field current-driven instabilities have been proposed to play an essential role in electron heating at shocks (Wu et al. 1984; Moses et al. 1985; Winske et al. 1987), even though Papadopoulos (1977) had earlier found that anomalous resistivity due to ion-acoustic and ion cyclotron instabilities preferentially heats the ions and to lesser extent the electrons. These early theoretical works originate from before sufficient quality measurements were available, which has left many problems related to shocks in an inconclusive state.

A novel stochastic heating mechanism was proposed by Balikhin, Gedalin & Petrukovich (1993) who suggested that the gradient of the macroscopic cross-shock electric field E_x could produce $\chi_e = (\omega_{ce}B)^{-1}\partial E_x/\partial x > 1$, which is a criterion for stochastic heating (Cole 1976; Karney 1979; McChesney, Stern & Bellan 1987) where nearby particle orbits deviate from each other exponentially with time. Here, $\omega_{ce} = eB/m_e$ is the angular electron cyclotron frequency. However, the cross-shock potential $\Delta\Phi$ and the resulting electric field $E_x = -\partial\Phi/\partial x$ and electric field gradient $\partial E_x/\partial x$ are too small to fulfil

★ E-mail: kstasiewicz@cbk.waw.pl (KS); bengt.eliasson@strath.ac.uk (BE)

the stochasticity condition, and this mechanism has been found by Scudder (1995) not to work for the parameters of the bow shock.

Another school of thought put more emphasis on electron energy increases due to the cross-shock electric potential and DC magnetic field. By using the Liouville mapping technique of electron distributions, Hull et al. (2001) and Lefebvre et al. (2007) suggested that no heating by waves is needed to explain observations at shocks.

On the contrary, after the analysis of THEMIS observations, Mozer & Sundqvist (2013) suggested that strong electrostatic waves $\widetilde{E} \sim 100\,\mathrm{mV\,m^{-1}}$ would demagnetize the electrons, which could then be heated by the DC cross-shock electric field. In addition, they noted that isotropization of the electron distribution and temperature $T_{e\parallel} \approx T_{e\perp}$ occurs instantaneously within the instrument accuracy, which requires strong interactions with waves. Isotropization cannot be accomplished by the DC adiabatic acceleration, which increases $T_{e\perp} \propto B$ only. However, their conclusions have been questioned by Schwartz (2014) who provided other arguments for the reported discrepancy, $T_e/B \neq T_{eu}/B_u$.

The situation described above has left four major problems unresolved: (i) the reason for deviations ($T_{e\perp}/B \neq$ constant) from adiabaticity, (ii) the role of stochastic heating by electrostatic waves at shocks, and (iii) the cause of rapid electron isotropization, and (iv) the role of the cross-shock potential. We do not consider here acceleration of electrons by parallel electric fields, addressed recently by Chen et al. (2018), which is rather well-understood.

1.1 Electron heating problem from magnetospheric multiscale perspective

Some of the above listed four points of controversy have recently been resolved with the help of four-point measurements by the Magnetospheric Multiscale (MMS) mission (Burch et al. 2016).

(i) *The reason for strong deviations $T_{e\perp}/B \neq$ constant*

The basic process at shocks is the betatron heating by the induction electric field ($\mathrm{curl}\,\mathbf{E} = -\partial\mathbf{B}/\partial t$) on increasing B observed in the convective frame, which is equivalent to adiabatic heating by conservation of the magnetic moment. For an arbitrary distribution of electrons, the adiabatic increase of perpendicular energy of each electron leads to an increase of average perpendicular energy (temperature) so that $T_{e\perp}/B =$ constant, contrary to claims made by Schwartz (2014). However, departures from this adiabatic behaviour have been reported by many authors (Scudder 1995; Mozer & Sundqvist 2013) and are observed in all shocks measured by MMS that we have analysed (Stasiewicz & Eliasson 2020a, b, 2021).

In most regions, electrons are heated adiabatically on the shock ramp, but small-scale oblique waves with finite $\widetilde{E}_\parallel$ redistribute the energy gain from two perpendicular directions $2dT_\perp$ into the parallel direction $dT_\parallel$ (Stasiewicz & Eliasson 2020a), breaking the conservation of magnetic moment. Conservation of energy leads to the following relation for isotropic electron temperature, which has been named quasi-adiabatic

$$T_e = T_{eu}\left(\frac{B}{B_u}\right)^{1+\alpha}, \tag{1}$$

with a theoretical value $\alpha = -1/3$ representing the departure from adiabaticity, $\alpha = 0$. In some quasi-perpendicular shocks $\alpha \approx -1/3$ has indeed been found (Stasiewicz & Eliasson 2020a), while some shocklets in quasi-parallel shocks exhibit even larger departure from adiabaticity, $\alpha \approx -2/3$ (Stasiewicz & Eliasson 2020b). As discussed in Section 2.2 below, $\alpha > 0$ is observed when the downstream temperature is higher than implied by adiabaticity, which may indicate additional stochastic heating.

(ii) *The role of stochastic heating by electrostatic waves*

At large gradients in the perpendicular electric field caused by electrostatic waves, the charged particle orbits can become unstable, leading to chaotic motion and very rapid 'stochastic heating' of the plasma particles. The criterion for stochastic energization has been recently generalized by Stasiewicz (2020) to the form

$$\chi_j(t,\mathbf{r}) = (\omega_{cj}B)^{-1}\mathrm{div}\,\mathbf{E}_\perp; \quad |\chi_j| > 1, \tag{2}$$

where $\mathbf{E}_\perp$ is the electric field component perpendicular to the magnetic field, and $\omega_{cj} = q_jB/m_j$ is the angular cyclotron frequency of particle species with charge q_j and mass m_j ($j = e$ for electrons, $j = p$ for protons, and $j = i$ for general ions). This criterion can be easily computed from MMS data and shows unambiguously that large amplitude electrostatic waves measured at shocks always fulfil the stochastic condition for protons, $\chi_p \gg 1$ (Stasiewicz & Eliasson 2020a), while waves in the frequency range 40–4000 Hz fulfil occasionally the stochastic condition for electrons, $\chi_e > 1$ (Stasiewicz & Eliasson 2020b). This can be easily verified by estimating the gradient of the electric field measured on two satellites, $\partial E_x/\partial x \approx (E_{x,1} - E_{x,2})/(x_1 - x_2)$. The computed values of χ_j are accurate for wavelengths >20 km because of the separation distance of the four MMS satellites. For shorter wavelengths, $\lambda \lesssim 20$ km, the computed values of div $\mathbf{E}$ and χ_e can be strongly underestimated.

When $\chi_e > 1$, stochastic heating is activated intermittently in localised regions which leads to large spikes in the ratio $T_{e\perp}/B \gg T_{eu}/B_u$. However, some of the spikes are produced by depressions of B, which are not accompanied by an adiabatic decrease of the temperature (Stasiewicz & Eliasson 2020b), possible due to the small size of these structures.

The stochastic heating mechanism has nothing in common with 'anomalous resistivity' mentioned above. Stochastic heating is a purely collisionless, single particle process which randomizes particle orbits within a fraction of the gyroperiod or a few wave periods, whichever is shorter. When $\chi_j > 1$, the perpendicular gyration velocity of a particle of species j can be increased by the $\widetilde{E} \times B$ velocity in the wave electric field as $\widetilde{V}_{E\times B} = \widetilde{E}_\perp/B$. The acceleration capacity of this mechanism is thus

$$v_\perp \sim v_{\perp 0} + \widetilde{E}_\perp/B, \tag{3}$$

where $v_{\perp 0}$ is the initial gyration velocity (or the thermal speed) of the particles.

Heating maps produced by Stasiewicz & Eliasson (2020a), Stasiewicz & Eliasson (2020b), and Stasiewicz & Eliasson (2021) show that heating of particles with cyclotron frequency f_c is most efficient by waves in the frequency range (0.1–5)f_c, and the wave vectors must fulfil the condition $k_\perp r_c \lesssim 12$, where r_c is the gyroradius. This means that the wavelengths should be on the order of the gyroradius or longer. This criterion excludes Debye length-sized waves and electrostatic structures, which may have large $\chi_e \gg 1$, but which have too short wavelengths for efficient electron and/or ion heating.

(iii) *The cause for rapid electron isotropization*

Simulations by Stasiewicz & Eliasson (2020b) show that obliquely propagating electrostatic waves with parameters derived from MMS observations at shocks can bring a disc-like perpendicular distribution to spherical isotropy within a few electron gyroperiods. Thus, perpendicular adiabatic heating of electrons is rapidly transferred by waves to the parallel direction conforming with observations of simultaneous parallel and perpendicular heating of electrons (Mozer & Sundqvist 2013).

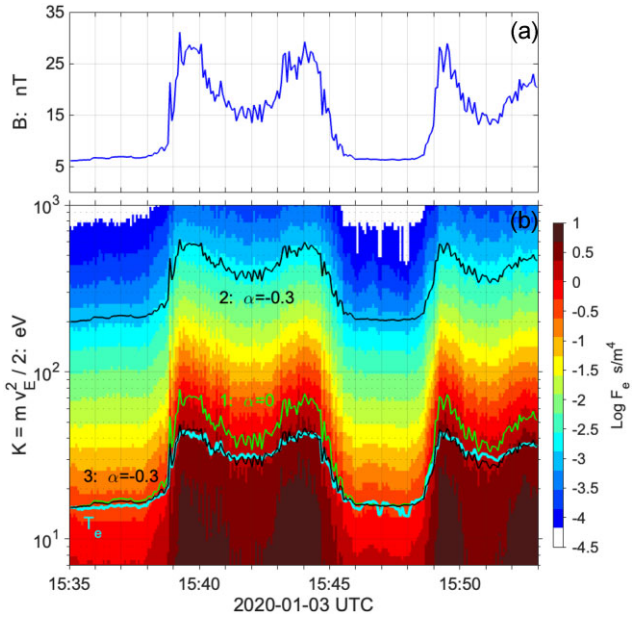

Figure 1. Three quasi-perpendicular shock crossings encountered by the MMS3 spacecraft on 3 January, 2020. (a) Magnetic field B resampled to 0.22 Hz. (b) One-dimensional (1D) electron distribution function $F(v_E, t)$ at 4.5 s time resolution. Overlaid are: the measured electron temperature $T_{e\perp}$ (cyan); line '1' – adiabatic mapping of $T_{e\perp u}$; line '2' – quasi-adiabatic mapping of the upstream energy 200 eV, line '3' – quasi-adiabatic mapping of $T_{e\perp u}$ by equation (1) with $\alpha = -0.3$.

In the following section we shall augment these findings by analysing two shocks where quasi-adiabatic and stochastic heating can be clearly identified. To illustrate the physical mechanisms involved in electron heating we perform also test-particle simulations in a realistic shock model containing a magnetic ramp and a cross-shock electric field.

2 EVIDENCE FOR QUASI-ADIABATIC AND STOCHASTIC ELECTRON HEATING

2.1 Quasi-adiabatic heating

On 2020 January 3, the MMS spacecraft encountered a series of eleven shock crossings during time 13:40–16:00 UTC caused by the oscillatory movement of the bow shock. The shocks had quasi-perpendicular orientation and were analysed in the context of ion energization and heating by Stasiewicz & Kłos (2022a), who give further background information about the observations. Fig. 1 shows the last three shock crossings from this event, at 15:39 UTC, 15:45 UTC, and 15:49 UCT, before the satellites finally entered the magnetosheath. The first shock at 15:39 UTC was encountered at position [9.2, 12.8, -2.0] R_E GSE (geocentric solar ecliptic), and the last shock at 15:49 UTC at position [9.1, 12.7, -2.0] R_E GSE. In the upstream position at 15:37 UTC the flow Alfvén Mach number was $V_i/V_A = 6.8$ and the plasma beta $\beta_i = 1.8, \beta_e = 1$. Here, V_A is the Alfvén speed. The angle between the ion flow velocity $\mathbf{V}_i$ and the magnetic field was $\angle_{VB} \approx 104^\circ$.

Fig. 1(a) shows the magnetic field B measured by the fluxgate magnetometer (Russell et al. 2016). It is resampled to the same frequency as the electron distribution function measured by fast plasma investigation (Pollock et al. 2016) and shown in panel b. The data are from fast survey mode where the electron distribution function was sampled during 4.5 s. The spectrogram represents the colour-coded reduced 1D electron distribution function $F(v_E, t)$ in velocity space $(v_{E\times B}, v_E, v_B)$, where the x-component is in the direction of the $E \times B$ drift, the y-component is along the perpendicular electric field, and the z-component is along the magnetic field. The 1D velocity distribution $F(v_E, t)$ is obtained by integrating the measured three-dimensional distribution function over the two other velocity dimensions $(v_{E\times B}, v_B)$. The vertical axis shows the kinetic energy $K = m_e v_E^2/2$ in place of v_E.

Over-plotted in Fig. 1(b) are: the measured electron temperature $T_{e\perp}$ (cyan line); line '1' – adiabatic mapping ($\alpha = 0$) of $T_{e\perp u}$ from 15:35 UTC; line '2' – quasi-adiabatic mapping ($\alpha = -0.3$) of the upstream energy 200 eV; line '3' – quasi-adiabatic mapping of $T_{e\perp u}$ with $\alpha = -0.3$. It can be seen that line '3' gives a very good approximation to the measured temperature, while the adiabatic mapping given by the green line '1' deviates from $T_{e\perp}$. This indicates that electron heating at quasi-perpendicular shocks is not adiabatic, but quasi-adiabatic, given by equation (1). Similar behaviour has been reported also by Mozer & Sundqvist (2013) in their Fig. 6 based on THEMIS data. Stasiewicz & Eliasson (2020a) have shown that $\alpha = -1/3$ results if one assumes that perpendicular energy gain from betatron heating is redistributed to the parallel direction through scattering by waves while conserving the total kinetic energy. Other shocks may have different values of α.

Quasi-adiabatic mapping of the upstream energy $K_u = 200$ eV shown with line '2' represents in fact the Liouville mapping. The distribution function should be constant along the particle trajectory. It can be seen that it is approximately constant if the particle energy evolves according to equation (1) with $\alpha = -0.3$.

2.2 Stochastic heating

On 2022 February 3 at time 03:22:22 UTC the MMS encountered the quasi-perpendicular bow shock at position [14.1, -2.9, 3.5], or $R = 14.8\,R_E$. In the upstream position at 03:22:38 UTC the plasma beta was: $\beta_i = 1, \beta_e = 0.2$, and the flow Alfvén Mach number 4. The angle between the ion flow velocity and the magnetic field was $\angle_{VB} \approx 86^\circ$. Fig. 2 shows a 14 s data interval taken in burst mode, in the same format as Fig. 1. The magnetic field B shown in panel a is resampled to 33 Hz, which corresponds to the sampling frequency of the electron distribution function shown in panel b. The measured electron temperature $T_{e\perp}$ is shown in cyan line, whereas the adiabatic mapping of the upstream temperature $T_{e\perp u}$ is shown with green '1' line.

In Fig. 1 the observed temperature was below the expected adiabatic projection, but in Fig. 2 the measured temperature is higher than expected from adiabatic heating, indicating a non-adiabatic process. Black dots show acceleration capacity of the shock given by equation (3) with $v_{\perp 0} = v_{Te}$. Two vertical black lines mark small intensifications of the temperature which can be associated with stochastic wave heating, because they occur in small depressions of B, where the adiabatic decrease should be observed instead. These signatures lead us to the conclusion that his case corresponds to stochastic heating of electrons. The stochastic heating is not expected to follow the scaling of equation (1), nevertheless the measured temperature conform quite well with quasi-adiabatic projection, $\alpha \approx +0.4$ (not shown).

Line '2' represents adiabatic projection of the upstream energy 200 eV. It appears to conform very well with Liouville mapping $F(K, t) =$ constant, when $K \propto B$. This observation provides further support for the stochastic $\widetilde{E} \times B$ wave acceleration mechanism. We recall that heating maps for this mechanism (Stasiewicz & Eliasson 2020a,

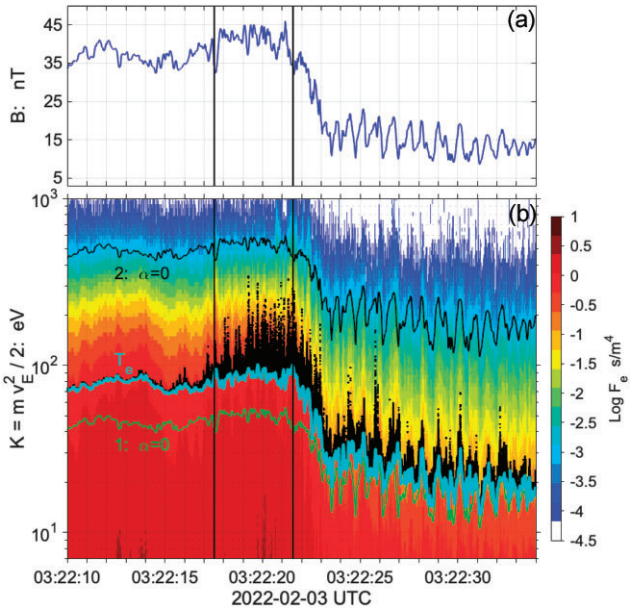

Figure 2. Quasi-perpendicular shock crossing observed in high-time resolution burst mode. (a) Magnetic field B resampled to 33 Hz. (b) 1D electron distribution function $F(v_E, t)$ at 0.03 s time resolution. Overlaid are: the measured electron temperature $T_{e\perp}$ (cyan); line '1' – adiabatic mapping of $T_{e\perp u}$; line '2' – adiabatic mapping of the upstream energy 200 eV. Black dots mark the acceleration capacity given by equation (3) for $v_{\perp 0} = v_{Te}$.

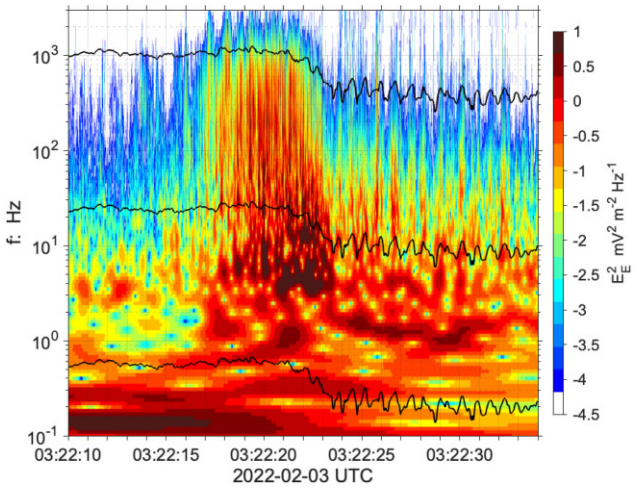

Figure 3. Time versus frequency power spectrogram for the $\widetilde{E}_E$ component of the electric field measured during time interval of Fig. 2. Black lines show the relevant frequencies: f_{ce} (upper line), f_{lh} (middle line), and f_{cp} (bottom line).

b, 2021) require $k_\perp r_c \lesssim 12$, which means $r_e/2 < \lambda_\perp$ for efficient stochastic heating. This implies that while the low energy electrons 0–10 eV have a small enough gyroradius r_e to be stochastically heated – the electrons from the tail of the distribution, $K > 100$ eV would have gyroradius too large and would not interact with waves. They would react adiabatically, $K \propto B$, which is observed indeed in Fig. 2, line '2'. We are not aware of any other mechanism that could account for the presented here observations.

2.2.1 *Waves that heat electrons*

Waves that heat electrons are measured by the double probe electric field experiments (Ergun et al. 2016; Lindqvist et al. 2016) in the frequency range 0–4096 Hz in burst mode. The spectrum of waves for the case of Fig. 2 is shown in Fig. 3 with three overlaid lines that mark plasma frequencies: f_{ce} – electron cyclotron frequency, f_{lh} – lower hybrid frequency, and f_{cp} – proton cyclotron frequency. The spectrum is computed for the wave electric field component $\widetilde{E}_E$ along the DC electric field determined from the ion drift velocity. For electrostatic waves in this direction the Doppler shift of frequency, $\mathbf{k}_\perp \cdot \mathbf{V}_\perp$, should be minimal.

Waves in the frequency range f_{cp}–f_{lh} are responsible for heating and acceleration of ions (Stasiewicz & Eliasson 2020a, 2021; Stasiewicz et al. 2021; Stasiewicz & Kłos 2022a, b), whereas waves at frequencies $f > f_{lh}$ have capacity to heat and accelerate electrons. They are also responsible for isotropisation of the electron distribution function (Stasiewicz & Eliasson 2020b). The wave electric field $\widetilde{E}$ in this bow shock reach a maximum amplitude of 200 mV m^{-1}, much larger than typical DC convection and cross-shock electric fields which are only a few mV m^{-1}.

The frequency spectrum in Fig. 3 shows proton cyclotron waves at f_{cp} near the bottom of the colour plot. The vertical striations extending to f_{ce} are caused by cascades of instabilities, which are presumably initiated by the diamagnetic current on the density compressions. The 'mother' frequency of these cascades appear to lie in the range 1–4 Hz, or several f_{cp}. We shall refrain here from identification of the wave modes and the instabilities involved, which requires deeper dedicated studies and separate publications. Waves at shocks in this frequency range have been already studied in numerous publications (Wilson III et al. 2010; Breneman et al. 2013; Wilson III et al. 2014; Mozer & Sundqvist 2013; Goodrich et al. 2018; Stasiewicz 2020; Stasiewicz & Eliasson 2020a, 2021; Stasiewicz et al. 2021; Stasiewicz & Kłos 2022a)

In the context of the electron heating by the $\widetilde{E} \times B$ wave mechanism we would like to stress that the stochastic perpendicular heating can be accomplished by waves in the frequency range from f_{lh} to $\sim 5 f_{ce}$, with a maximum efficiency around f_{ce}, as implied from the above mentioned heating maps. In the case of Figs 2 and 3 the thermal electron gyroradius is $r_e \approx 1$ km, whereas the hybrid gyroradius $r_h = (r_e r_p)^{1/2} \approx 10$ km. For thermal electrons with gyroradius $r_e \approx 1$ km the stochastic heating requires wavelengths $\lambda_\perp > 0.5$ km. It is likely that the electron heating is accomplished by waves in the range r_e–r_h, i.e. $\lambda_\perp = 1$–10 km in this particular case. This represents a prediction of our model, which cannot be directly verified with MMS measurements. The spacecraft separation which is on average 34 km in this case does not make it possible to properly resolve kilometre-length waves and would produce strongly underestimated values for χ_e.

3 TEST-PARTICLE SIMULATIONS

To help understand the physical mechanisms involved in electron heating we here carry out test-particle simulations in a realistic shock model containing a magnetic ramp and a cross-shock electric field. Let us assume that the convection electric field E_y convects plasma $V_x = E_y/B$ through the magnetic field $\mathbf{B}(x') = [0, 0, B_z(x')]$ of a perpendicular shock with thickness D, located at the physical coordinate $x' = 0$ and described by the magnetic profile

$$\frac{B_z(x')}{B_u} = g(x') = \frac{c_r - 1}{2}\tanh\left(\frac{x'}{D}\right) + \frac{c_r + 1}{2}, \quad (4)$$

where $c_r = B_d/B_u$ is the compression ratio between the downstream and upstream values. We assume also the cross-shock electric field

implied by the generalized Ohm's law of the two-fluid equations

$$E_{sx}(x') = -\frac{1}{eN}\frac{\partial p_e}{\partial x'}, \tag{5}$$

where $p_e = NT_e$ is the electron pressure, N is the number density, T_e the electron temperature in energy units, and e is the electron charge. Electrostatic waves, $\mathbf{E}_w \sin(\omega_d t' - \mathbf{k}\cdot\mathbf{r}')$, are generated inside the shock ramp and propagate at angle ϕ to the x direction and angle θ to the z direction with the Doppler-shifted frequency ω_d in the observer's (shock) frame.

The position $\mathbf{r}'$ and velocity $\mathbf{v}$ of a particle with mass m and charge q are determined by the equation $m\mathrm{d}\mathbf{v}/\mathrm{d}t' = q(\mathbf{E} + \mathbf{v}\times\mathbf{B})$ together with $\mathrm{d}\mathbf{r}'/\mathrm{d}t' = \mathbf{v}$. By using dimensionless variables with time t' normalized by ω_c^{-1}, space by $k_\perp^{-1}$ and velocity by $\omega_c/k_\perp$ (with $\omega_c = |q|B_u/m$ being the angular cyclotron frequency in the upstream side), the normalized equations of motion for a test ion or electron in the shock frame are

$$\pm\frac{\mathrm{d}u_x}{\mathrm{d}t} = u_y g(x) + \chi_{sx}(x) + (\chi_w\cos\phi)\sin\Psi, \tag{6}$$

$$\pm\frac{\mathrm{d}u_y}{\mathrm{d}t} = -u_x g(x) + Mu_{\perp 0} + (\chi_w\sin\phi)\sin\Psi, \tag{7}$$

$$\pm\frac{\mathrm{d}u_z}{\mathrm{d}t} = (\chi_w\kappa)\sin\Psi, \tag{8}$$

$$\frac{\mathrm{d}x}{\mathrm{d}t} = u_x; \quad \frac{\mathrm{d}y}{\mathrm{d}t} = u_y; \quad \frac{\mathrm{d}z}{\mathrm{d}t} = u_z, \tag{9}$$

were the negative sign applies for electrons. Here, $\Psi = \Omega_d t - x\cos\phi - y\sin\phi - \kappa z$ is the wave phase with the Doppler-shifted angular frequency $\Omega_d = \omega_d/\omega_c = \Omega + u_d\cos\phi$ with respect to $\Omega = \omega/\omega_c$ in the plasma frame, $u_d = Mu_{\perp 0}/g(x)$ is the normalized convection velocity, and $\kappa = k_z/k_\perp = E_{wz}/E_{w\perp} = \cos\theta/\sin\theta$. Parameter $M = E_y/(B_u v_{0\perp})$ is the 'thermal' Mach number of the upstream convection velocity E_y/B_u. The initial gyration velocity of the particle in the upstream region is $u_{0\perp} = v_{0\perp}k_\perp/\omega_c = k_\perp r_c$, where $r_c = v_{0\perp}/\omega_c$ is the gyroradius. The normalized amplitude of the wave electric field is

$$\chi_w = \frac{E_{w\perp}}{B_u}\frac{k_\perp}{\omega_c} = \frac{E_{w\perp}}{E_y}Mu_{\perp 0}, \tag{10}$$

which represents also the wave stochastic parameter (2).

The function $\chi_{sx}(x)$ with $x = x'k_\perp = x'u_{\perp 0}/r_c$ corresponds to the normalized cross-shock electric field (5) in the form

$$\chi_{sx}(x) = \frac{E_{sx}}{B_u}\frac{k_\perp}{\omega_c} = \frac{-\chi_s u_{\perp 0}}{\cosh^2(x/k_\perp D)}, \tag{11}$$

where $k_\perp D = u_{\perp 0}D/r_c$, and

$$\chi_s = \frac{\omega_{ce}}{\omega_c}\frac{r_{Te}}{r_c}\frac{r_{Te}}{D}\frac{(c_r-1)}{2}, \tag{12}$$

with $r_{Te} = v_{Te}/\omega_{ce}$ being the thermal electron gyroradius in the upstream position. This is derived from equation (5) assuming that both $N = N_u g(x)$ and $T_e = T_{eu}g(x)$ behave as B in equation (4), which are empirical relations observed at quasi-perpendicular shocks. Note also that $N \propto B$ and $V_x = E_y/B$ ensure the flux continuity equation $NV_x =$ constant in the present shock potential model.

Equations (5) and (11) can be integrated to give the cross-shock potential in physical variables

$$\Phi_s(x') = \frac{(T_{ed}-T_{eu})}{e}[\tanh(\frac{x'}{D}) + 1], \tag{13}$$

with a maximum potential drop $\Delta\Phi_s = 2(T_{ed} - T_{eu})/e$, which is typically about 150 V.

The parameters controlling the solutions of equations (6)–(9) are the shock parameters $c_r = B_d/B_u, r_c/D$, the Mach number M, the shock electric field amplitude χ_s, the wave parameters $\Omega, k_\perp, \kappa, \chi_w$, and the initial velocity or gyroradius $u_{\perp 0} = k_\perp r_c$.

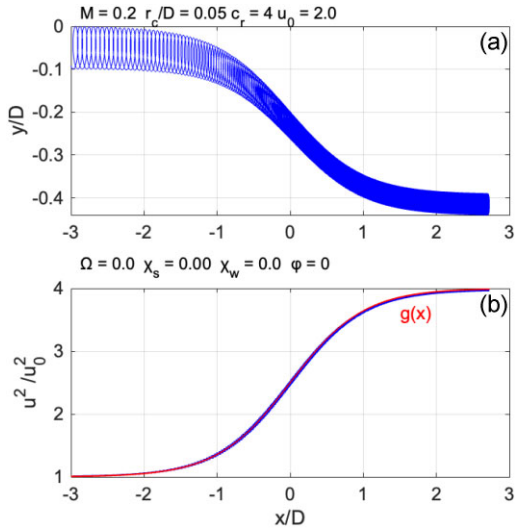

Figure 4. Electron drift across the shock without the cross-shock potential and waves, $\chi_s = \chi_w = 0$. (a) electron trajectory in the (x, y) plane normalized by the thickness D of the shock. In panel (b) the normalized gyration energy $u^2(x)/u_{\perp 0}^2$ follows exactly the magnetic field $g(x) = B/B_u$, indicating adiabatic behaviour.

The initial gyration kinetic energy of a particle is determined by the value r_c/λ, where λ is the wavelength. In case of the absence of waves, $\chi_w = 0$, all equations are still valid, but $u_{\perp 0}$ becomes an arbitrary scaling parameter for the velocity which removes the dependence on the undefined $k_\perp$. The initial energy of the particle is then determined by the ratio r_c/D.

3.1 Equivalence of adiabatic heating and gradient B drift acceleration

We use typically observed parameters at shocks to compute the dimensionless parameters in equations (6)–(9): $r_e \approx 2$ km, $D = 50$ km, shock compression ratio $c_r = 4$, and the Mach number $M = 0.2$, which corresponds to the solar wind perpendicular speed 400 km s^{-1} and the upstream thermal velocity 2000 km s^{-1} of a 12 eV electron.

In the first simulation run shown in Fig. 4, the electron drifts through the shock without waves and with a zero cross-shock potential, $\chi_w = \chi_s = 0$. Electron executes electric drift $V_x = E_y/B$ and gradient B drift $V_y = -(\mu/eB)\mathrm{d}B/\mathrm{d}x$ with

$$\mu = \frac{mv_\perp^2}{2B}, \tag{14}$$

being the magnetic moment. Magnetic gradient drift moves the particle across the electric equipotentials increasing gyro-motion energy

$$\frac{mv_\perp^2}{2} = \frac{mv_{\perp 0}^2}{2} + q(y-y_0)E_y, \tag{15}$$

which represents gradient B drift energization by the convection electric field. In this drift process, the magnetic moment μ is a constant of motion (Northrop 1963) and represents adiabatic heating on increasing B. Using that $mv_\perp^2/2B = mv_{\perp 0}^2/2B_u$ to eliminate $v_\perp^2$ in equation (15) gives the trajectory of the gyrocentre in the x–y plane

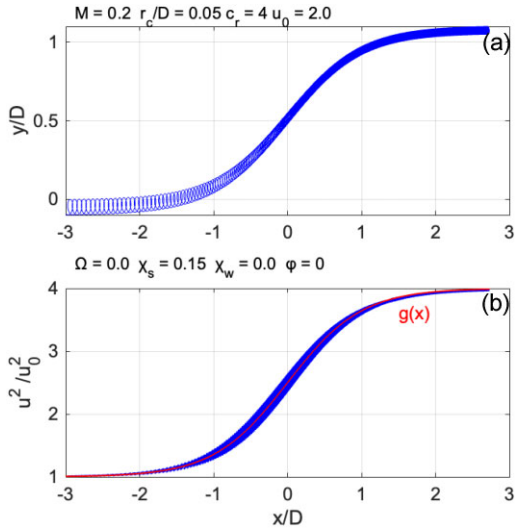

Figure 5. The same as in Fig. 4 but with the cross-shock electric field, $\chi_s = 0.15$.

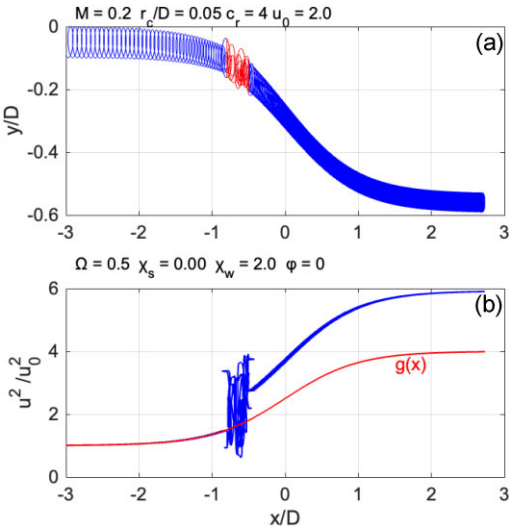

Figure 6. The same as in Fig. 4 but with the wave electric field at frequency $\omega = 0.5\,\omega_c$ and amplitude $\chi_w = 2$. Waves are active only in a small region marked red in panel (a).

as

$$\frac{mv_{\perp 0}^2}{2}\left(\frac{B(x)}{B_u}-1\right) = q(y-y_0)E_y, \tag{16}$$

which coincides with the particle simulation trajectory in Fig. 4(a). The limiting value for the perpendicular energy (temperature) increase is $T_d/T_u = B_d/B_u$ as seen in Fig. 4(b). This shows that gradient B drift heating on convection electric field is equivalent to adiabatic heating on increasing B driven by convection. This applies only to particles with low Mach numbers, $M < 1$. Low energy particles with higher Mach numbers make negligible drift, but are still adiabatically heated.

3.2 Effects of the cross-shock potential

It has been postulated that the cross-shock potential could contribute to the electron heating. To investigate this problem we make the second run depicted in Fig. 5 by adding the cross-shock electric field (11) with amplitude $\chi_s = 0.15$. It can be seen that the primary effect of E_{sx} directed sunward is to cause a convection drift that opposes gradient B drift. This additional drift changes considerably the electron path through the shock as can be seen in Figs 4 and 5. In panel (b) we see that the adiabatic heating is not affected by this field. This holds in cases when the gradient of this field is below the stochastic threshold, i.e. $(\omega_c B)^{-1}\partial E_{sx}/\partial x < 1$.

It should be emphasized that the above simulations apply to an ideal situation when there are no waves that scatter and isotropize electrons. In the presence of waves which do not exceed the stochastic threshold (2), the quasi-adiabatic relation (1) applies with $\alpha \approx -1/3$, which is observed in measurements shown in Fig. 1.

3.3 Stochastic wave acceleration

Fig. 6 shows a run including a wave electric field of amplitude $\chi_w = 2$, above the stochastic threshold and localized in a small region inside the ramp marked red in panel (a). It is seen in panel (b) that waves at frequency $\omega = 0.5\omega_c$ can easily lift the heating ratio to 6 in this particular case, well above the adiabatic compression $c_r = 4$. The wave stochastic heating would produce positive α in $T_{e\perp} \propto B^{1+\alpha}$, what is observed in Fig. 2. The interaction is chaotic in nature, i.e. it strongly depends on initial conditions. The efficiency of stochastic wave heating for various parameters can be inferred from heating maps published by Stasiewicz & Eliasson (2020a), Stasiewicz & Eliasson (2020b), Stasiewicz & Eliasson (2021). The acceleration limit is given by (3), about 1 keV for electrons, which is supported by measurements in Fig. 2. Because the wave electric field $\sim$100 mV m^{-1} is much larger than the convection and the cross-shock electric fields, which are a few mV m^{-1}, the stochastic wave acceleration, if activated, would dominate other types of acceleration.

4 CONCLUSIONS

We have demonstrated that measurements obtained from MMS mission support quasi-adiabatic relation $T_{e\perp} \propto B^{1+\alpha}$, where α represents departure from adiabaticity. Negative $\alpha < 0$ is observed in most situations, when the threshold for stochastic heating of electrons is not exceeded, or waves do not have wavelengths that facilitate stochastic heating. Perpendicular energy gain from betatron heating is then redistributed by interactions with waves to the parallel direction leading to a lower isotropic temperature increase. Positive α is observed when the stochastic heating of electrons is activated by the $\widetilde{E} \times B$ wave acceleration mechanism leading to a higher temperature increase.

To illustrate the physical mechanisms involved, test-particle simulations were carried out in a realistic shock model containing a hyperbolic tangent magnetic profile and a cross-shock electric field created by the electron pressure. It was shown that adiabatic betatron heating is in fact equivalent to the gradient B drift acceleration in a convection electric field. It was found that the cross-shock electric field has no effect on electron heating but it affects the electron path through the shock. On the contrary, the stochastic wave acceleration process can easily explain the observations, when the electron heating is stronger than adiabatic, which manifests as a positive α in quasi-adiabatic relation (1). We have concluded that waves responsible for electron heating should have frequencies above the lower hybrid frequency up to the electron cyclotron frequency and wavelengths longer than half the electron gyroradius. The process of betatron/gradient B heating and signatures of quasi-adiabatic heating,

and stochastic heating of electrons are observed in all shocks that we have analysed with measurements by the MMS.

ACKNOWLEDGEMENTS

This work has been supported by the National Science Centre (NCN), Poland, through grant No. 2021/41/B/ST10/00823. BE acknowledges support from the EPSRC (UK), grants EP/R004773/1 and EP/M009386/1.

DATA AVAILABILITY

The data supporting the results in this article are available through the MMS Science Data Center at the Laboratory for Atmospheric and Space Physics (LASP), University of Colorado, Boulder: https://lasp.colorado.edu/mms/sdc/public/.

The data have been processed with the IRFU-Matlab analysis package available at https://github.com/irfu/irfu-matlab.

REFERENCES

Balikhin M., Gedalin M., Petrukovich A., 1993, Phys. Rev. Lett., 70, 1259
Bame S. J., Asbridge J. R., Gosling J. T., Halbig M., 1979, Space Sci. Rev., 23, 75
Breneman A. W., Cattell C. A., Kersten K., Paradise A., Schreiner S., Kellogg P. J., Goetz K., Wilson L. B. III, 2013, JGR, 118, 7654
Burch J. L., Moore R. E., Torbert R. B., Giles B. L., 2016, Space Sci. Rev., 199, 1
Chen L.-J. et al., 2018, Phys. Rev. Lett., 120, 225101
Cole K. D., 1976, Planet. Space Sci., 24, 515
Ergun R. E. et al., 2016, Space Sci. Rev., 199, 167
Goodrich K. A. et al., 2018, J. Geophys. Res., 123, 9430
Hull A. J., Scudder J. D., Larson D. E., Lin R., 2001, J. Geophys. Res.: Space Phys., 106, 15711
Karney C. F. F., 1979, Phys. Fluids, 22, 2188
Lefebvre B., Schwartz S. J., Fazakerley A. F., Décréau P., 2007, J. Geophys. Res.: Space Phys., 112, A09212
Lindqvist P. A. et al., 2016, Space Sci. Rev., 199, 137
McChesney J. M., Stern R., Bellan P. M., 1987, Phys. Rev. Lett., 59, 1436
Moses S. L., Coroniti F. V., Kennel C. F., Scarf F. L., 1985, Geophys. Res. Lett., 12, 609
Mozer F. S., Sundqvist D., 2013, J. Geophys. Res., 118, 5415
Northrop T. G., 1963, The Adiabatic Motion of Charged Particles, Interscience Publishers, New York
Papadopoulos K., 1977, Rev. Geophys., 15, 113
Pollock C. et al., 2016, Space Sci. Rev., 199, 331
Russell C. T. et al., 2016, Space Sci. Rev., 199, 189
Schwartz S. J., 2014, J. Geophys. Res.: Space Phys., 119, 1507
Scudder J., 1995, Adv. Space Res., 15, 181
Scudder J. D., Lind D. L., Ogilvie K. W., 1973, J. Geophys. Res., 78, 6535
Stasiewicz K., 2020, MNRAS, 496, L133
Stasiewicz K., Eliasson B., 2020a, ApJ, 903, 57
Stasiewicz K., Eliasson B., 2020b, ApJ, 904, 173
Stasiewicz K., Eliasson B., 2021, MNRAS, 508, 1888
Stasiewicz K., Kłos Z., 2022a, Ann. Geophys., 40, 315
Stasiewicz K., Kłos Z., 2022b, MNRAS, 513, 5892
Stasiewicz K., Eliasson B., Cohen I. J., Turner D. L., Ergun R. E., 2021, J. Geophys. Res.: Space Phys., 126, e2021JA029477
Thomsen M. F., Mellott M. M., Stansberry J. A., Bame S. J., Gosling J. T., Russell C. T., 1987, J. Geophys. Res.: Space Phys., 92, 10119
Wilson III L. B., Cattell C. A., Kellogg P. J., Goetz K., Kersten K., Kasper J. C., Szabo A., Wilber M., 2010, J. Geophys. Res., 115, A12104
Wilson III L. B., Sibeck D. G., Breneman A. W., Le Contel O., Cully C., Turner D. L., Angelopoulos V., Malaspina D. M., 2014, J. Geophys. Res., 119, 6475
Winske D., Giacalone J., Thomsen M. F., Mellott M. M., 1987, J. Geophys. Res.: Space Phys., 92, 4411
Wu C. S., Zhou Y. M., Tsai Shih-Tung, Guo S. C., Winske D., Papadopoulos K., 1984, Space Sci. Rev., 37, 63

This paper has been typeset from a TEX/LATEX file prepared by the author.